Journal Home Page: https://sjes.univsul.edu.iq

Research Article:

"Nonlinear Finite Element Modeling of Shear Behavior of Concrete Deep Beams Reinforced with Internal Glass Fiber-Reinforced Polymer Bars by ANSYS"

Shuaaib Abdalla Mohammed [1,a,*]
Serwan Khurshid Rafiq[2,a]
Zana Abdalla Aziz[3,a]
[a] University of Sulaimani, College of Engineering, Civil Engineering Department

Article Information

Article History:
Received September 14th 2021
Accepted : 11th October 2021
Available online: December 31st , 2021

Keywords:
Deep beams; fiber-reinforced polymer bars; failure mechanisms; shear span-depth ratio (a/d).

About the Authors:

Corresponding author:
Shuaaib Abdalla Mohammed
E-mail: shuaaib.mohammed@univsul.edu.iq
Researcher Involved:
Asst. Prof. Dr. Serwan Khurshid Rafiq
Zana Abdalla Aziz

DOI https://doi.org/10.17656/sjes.10149

Abstract

The purpose of this paper is to numerically trace the behavior of concrete deep beams reinforced with internal Glass Fiber-Reinforced Polymer (GFRP) bars and containing no web reinforcement by using ANSYS program. For this purpose, a finite element model is used for concrete deep beams that previously examined in an experimental study and its predicted failure loads were compared with the actual failure loads. The results of the finite element model were in a good agreement with observations from the experimental study. The comparisons showed that the used model has the ability to capture the shear behavior, as well as load-deflection response and crack patterns of deep beams reinforced with internal GFRP bars in the entire range of loading. The paper is also covered a parametric study on shear span-to-depth (a/d) ratio, GFRP reinforcement ratio and concrete compressive strength which they usually have high impacts on the behavior of fiber-reinforced concrete beams. The results of the parametric study showed that the ultimate failure load of beams reinforced with GFRP bars was higher than that of steel-reinforced concrete beams. The maximum failure load was observed to decrease by decreasing the a/d ratio. The stiffness and ductility of the beams were increasing by increasing the reinforcement ratio.

1. Introduction

Concrete reinforced with steel bars is a common material used in structures for many decades and many researches have been carried out to study the structural behavior of such structures. However, the steel reinforcement corrosion has been identified as a cause of additional costs due to the maintenance of such structures exposed to aggressive environments. Besides the costly solutions such as epoxy coating of reinforcing bars or using concrete admixtures, as a cost effective technique to fight against corrosion, FRP bars are being increasingly used currently to replace the old-type steel reinforcement in such structures due to their non-corrodible characteristics [1]. Some other advantages of FRPs are easy to install and generally improve the ductility of concrete beams [2]. They are also useful in structures need magnetic transparency and in members which might be subjected to chemical attacks [3]. There are many developed design procedures to document the shear response of steel-reinforced concrete members [4, 5]. The shear behavior of slender fiber-reinforced concrete beams has been also investigated by many researches [6-8]. However, little attention has been given to deep beams with shear span-to-depth ratio of less than 2.0 reinforced with longitudinal FRP bars and without web reinforcements [9]. Deep Beams are mainly used as girders in multi-story buildings, highway bridges, coupling beams of shear walls and as pile caps due to their high shear capacity. The results of many studies show that the shear behavior such as shear strength, deformation, and cracks width of FRP-deep beams is different from that of deep beams reinforced with conventional steel [10-12]. Usually, strut-and-tie method is recommended by many codes of practice to be used for the analysis and design of reinforced concrete beams, while using

strut-and-tie modeling is not permitted by FRP design codes [13]. Therefore, several design codes for reinforced concrete construction recommends different numerical models to evaluate the shear strength of deep beams. [14, 15]. In this paper, a numerical program has been undertaken to predict the shear behavior of concrete deep beams internally reinforced with GFRP bars. The modeling technique also has been validated by comparing the obtained results of this work to the results from the selected experimental study [16]. In order to enhance the durability of structures exposed to aggressive environments, internal FRP bars has been used in such structures. Several members within these structures may have disturbed regions due to the nonlinear strain distribution. More research is needed to investigate the performance of such members, deep beams in particular, containing these disturbed regions. This research program was carried out to study the shear response of internally reinforced concrete deep beams with GFRP and without shear reinforcement using ANSYS Program. The study also covers several parameters includes span to depth ratio, the GFRP reinforcement ratio, specified concrete compressive strength and the size of meshing.

2. Finite Element Modelling

In order to verify the applicability of the developed program to predict the shear capacity of internally reinforced deep beams with GFRP bars, a numerical model was implemented in ANSYS (ANSYS 14.5). The response of reinforced concrete deep beams before cracking can be well predicted by linear elastic analysis, while nonlinear analysis should be used to evaluate their performance after cracking due to a major redistribution of stresses [17]. Nonlinear behavior of concrete and GFRP bars materials were considered in the finite element model. The load control technique was also used in the analysis by incrementing the loads in steps on the beam model until the attainment of failure. The configuration and geometry of the tested beams are adapted from an experimental study conducted by Matthias, et al [16]. The model was validated against the experimental measured responses using one specimen, designated as B1N, which was tested under major shear loading. The beam configuration, details of its reinforcement and material properties are shown in Fig. (1) and Table (1), respectively. The normal-strength concrete with specified 28-day strength of 40.5 MPa was used. Commercially available GFRP bars in size of 19 mm (No. 6) were selected for the type of longitudinal reinforcement in the specimen, as they are mostly used in the industry. There are three layers of reinforcement with 8 bars in the beam. Side and bottom clear cover were assumed to be 40 mm. The beam was tested under two-point loads applied at a distance of 250 mm on both sides of mid-span as shown in Fig. (1). A solid 65 element type has been used to model the concrete material in the finite element models. This type of element, shown in Fig. (2), can be frequently employed for the finite element modeling of solids in engineering practices. The element has eight nodes with three degrees of freedom and it can be used to model several three-dimensional solids elements. It is also able to account the concrete cracking in tension and crushing in compression [18]. The modulus of elasticity of concrete was calculated by equation (1) [15]:

$$Ec = 4700 \sqrt{f'c} \quad \ldots\ldots\ldots\ldots\ldots\ldots\ldots (1)$$

The stress-strain curve of concrete in compression has a linear form up to approximately one-third of the ultimate compressive strength. Then the stress gradually increases until reaches the ultimate compressive strength. Beyond the ultimate compressive strength, the curve falls into a softening region and crushing eventually occurs at ultimate strain. In this study, the concrete was also assumed to be homogenous and isotropic. The isotropic stress-strain curve for concrete can be computed by using the following equations:

$$f_c = \varepsilon E_c \quad \text{for } 0 \le \varepsilon \le \varepsilon 1 \ldots\ldots\ldots (2)$$

$$f_c = \frac{\varepsilon E_c}{1+\left(\frac{\varepsilon}{\varepsilon_o}\right)^2} \quad \text{for } \varepsilon 1 \le \varepsilon \le \varepsilon o \ldots\ldots\ldots (3)$$

$$f_c = f_c' \quad \text{for } \varepsilon o \le \varepsilon \le \varepsilon cu \ldots\ldots\ldots (4)$$

$$\varepsilon 1 = 0.3\, f_c'/Ec \ldots\ldots\ldots\ldots\ldots (5)$$

$$\varepsilon o = 2\, f_c'/Ec \ldots\ldots\ldots\ldots\ldots (6)$$

A simplified compressive uniaxial stress-strain curve, shown in Fig. (3) was adopted as required in ANSYS program to model the stress-strain relationship of concrete in compression. A LINK180 element type, shown in Fig. (4), was used to model the steel and GFRP bars and perfect bond between the concrete and reinforcing bars was assumed. This type of element has two nodes with three degrees of freedom, and it is able to model the plastic deformation. The steel material was assumed to be identical in both tension and compression and linear elastic properties was assumed for GFRP bars. The steel and GFRP stress-strain curve used in the finite element modeling is shown in Fig. (5). Generally, finite element models analyzed by providing fine mesh yield high accurate results. Therefore, to obtain accurate results, a relatively fine mesh is assigned to all elements of the finite element models. Fig. (6) shows a typical mesh of the finite element model of a beam specimen.

3. Model Validation

In order to illustrate the validity of the developed model in predicting the shear behavior of concrete deep beam, the load-deflection response of beam B1N was compared to the experimental results as shown in Fig. (7). Different stages of its response such as elastic stage with tensile cracking initiation, post-cracking stage and propagations of cracks followed by failure can be seen from the shown curve. The curve has a linear form before cracking with a constant slope, and it takes a nonlinear form after cracking. In general, the overall trend of the load-deflection behavior of the finite element model is in a good agreement with the experimental results in the pre- and post-cracking stages. In the elastic region, the load-deflection curve of the finite element model is slightly stiffer compared to that of experimental beam. The presence of micro-cracks in the experimental beam concrete due to drying shrinkage, which reduces the beam stiffness, can be the main cause of this difference as the finite element model does not consider micro-cracks. However, the finite element model shows a lower response in the post-cracking stage in comparison to the measured experimental response. This difference might be due to the idealization of mechanical properties of concrete and reinforcing bars in the finite element models, and due to the loading configuration and boundary conditions in practice. In addition, assuming a perfect bond between the concrete and reinforcement bars might not be correct compared to reality, partly due to the bond slippage. The same result was obtained in a study carried out by Ibrahim, et al [19]. In general, the overall stiffness of the finite element models is expected to be higher than that of experimental beams stiffness. The finite element model can also predict the propagation of cracks. In ANSYS, the crack locations and crushing of concrete are displayed by small circles with different colors. The crack pattern obtained by ANSYS program for the beam model is shown in Fig. (8). At first, the tested beam experienced vertical flexural cracks started at its extreme tension fibers under shear loading due to the concentration of tensile stresses near the mid-span. Then, as the load is further increasing, the main diagonal cracks initiated near the inside face of the supports and extended toward the points of load applications (compression zone) due to the increasing of shear stresses. These cracks became horizontal near the load-application points. At failure, more cracks were occurred and propagated in compression zone and the concrete is crushed between the loading points. This type of failure is usually referred to as flexural compression failure. The same cracking behavior was observed in the experimental work as shown in Fig. (9). In general, the crack pattern obtained in the nonlinear analysis is in a good agreement with the experimental results.

4. Results and Discussion

To see the effectiveness of using GFRP bars in concrete deep beams, a concrete beam reinforced with internal GFRP bars was compared to a steel-reinforced concrete beam. Fig. (10) shows the response of the finite element models with GFRP and steel reinforcement. The performance of the beam having GFRP bars was almost similar to that having steel reinforcing bars. The GFRP-reinforced beam however experienced larger deflection in comparison to the steel-reinforced beam. Such behavior is mainly due to the relatively low modulus of elasticity of GFRP bars. On the other hand, according to the figure, the maximum failure load of GFRP-reinforced beam was higher than that of beam reinforced with steel bars by 48% approximately. This increase might be attributed to the improvement in the arch action mechanism due to the high-resistance of GFRP to tension forces. In addition, the beam with GFRP experienced a more ductile failure in comparison to the beam having steel-reinforced bars. This result is in agreement with other research findings which stated that using of FRP in reinforced concrete members is an effective way to enhance their ductility [2, 6, 9]. The summary of results of GFRP-reinforced beams and steel-reinforced beams is shown in Table (2). In the finite element modeling, three span-to-depth ratios of 0.9, 1.08 and 1.19 were also taken to find out how the beam responses if the a/d ratio changes. The responses of the beams with different a/d ratios are shown in Fig. (11). It was found that changing the a/d ratio exhibited influential impacts on the shear strength of the tested beam. Referring to the figure, the ultimate load of the beam had dramatically dropped from 1098 kN to 889 kN by decreasing the a/d ratio from 1.08 to 0.9 and it has increased to 1100 kN with increasing the a/d ratio to 1.19. This might be mainly due to the penetration of the cracks at the top of the beam near the loading points as the failure mechanism is mainly affected by the a/d ratio as shown in Fig. (12). The mid-span deflection of beams was also observed to increase by increasing the a/d ratios as depicted in Fig. (11). This increase might be associated with exhibiting more diagonal cracking as the a/d increases. The same finding is observed in the work done by Abed, et al [11]. Also, in order to study the effects of reinforcement ratio, three different ratios of 1.41%, 1.74% and 2.32% were taken into consideration. Fig. (13) shows the response of the tested beam with the previously mentioned reinforcement ratios. The shear strength of the beam was found to be improved by increasing in the ratio of reinforcement. This improvement in shear strength might be attributed to the increase in compression block depth at failure. Increasing the reinforcement ratio by only 0.33% also results in 15% increase in the beam load-carrying capacity. In addition, the beam

with higher reinforcement ratio also showed stiffer response compared to beams with lower reinforcement ratio. The same observation was also found in a analytical study conducted by Chattopadhyay et al [20]. On other hand, the ductility of the beam was slightly decreased by increasing the amount of reinforcement. This is mainly due to the lower modulus of elasticity of the GFRP bars. The summary of the study of effects of reinforcement ratio is shown in Table (3). In addition, to understand the effects of compressive strength of concrete, different values of compressive strengths were taken in the numerical analysis. According to the results shown in Fig. (14), concrete compressive strength has a great impact on the beam's strength. From the load-deflection curve of the beam with different compressive strengths, it can be observed that the load-carrying capacity of the beam is increasing when the concrete compressive strength increases. The failure loads were (1010, 1100, and 1285) kN with compressive strength of (30, 40.5, and 50) MPa respectively. The model with compressive strength of 50 MPa achieved a 17% higher failure load compared to the beam model having the compressive strength of 40.5 MPa. The same response is observed for beams with different a/d ratios as shown in Fig. (15) and Fig. (16). Finally, the effects of compressive strength on the reinforcement stress are also studied. The reinforcement stresses for beams with different concrete compressive strengths are shown in Fig. (17) to Fig. (19). According to the figures, the reinforcement stresses in the entire length of GFRP bars were increased by increasing in concrete compressive strength. 52% and 25% increases are recorded in reinforcement stresses at beams mid-span by increasing the compressive strength from 30 to 40.5 MPa and 50 MPa, respectively.

5. Conclusion

Based on the results obtained from the finite element modeling, the following conclusion can be made: Nonlinear finite element modeling using ANSYS is able to simulate the shear behavior of deep beams reinforced internally with GFRP bars. The finite element model results also correspond well with the observed experimental data such as crack patterns and load-deflection behavior. Failure load of GFRP-reinforced beam was higher than that of steel-reinforced beam by 48%. Using GFRP was not only improve the maximum load-carrying capacity of the tested beam, but also enhance their ductility. A 20% decrease in the ultimate load of the tested beam was observed by decreasing the a/d ratio from 1.08 to 0.9. Increasing the reinforcement ratio resulted in increasing the shear cracking load and the failure load due to the increasing of concrete tensile strength. A 15% increase in shear strength is observed by increasing the reinforcement ratios from 1.41% to 1.74%. Shear strength of the concrete deep beams highly affected by concrete compressive strength. The ultimate load-carrying capacity was increased from 1100 kN to 1285 kN with increasing the concrete compressive strength from 40.5 MPa to 50 MPa. The reinforcement stresses were also increased by increasing the concrete compressive strength. Finally, it can be concluded that, the developed finite element model in this paper can be used to study the shear behavior of concrete deep beams reinforced with internal GFRP bars.

References

1. Hota V.S. GangaRao, N.T., P.V. Vijay., *Reinforced concrete design with FRP composites*. 2007, USA: CRC Press;.
2. Tabish Izhar, Q.R., *Fibre Reinforced Polymer Bars as main Reinforcement in Columns and Beams-A Review*. Journal of Emerging Technologies and Innovative Research, 2019. **6**(1): p. 174-178.
3. Balendran RV, R.T., Maqsood T, Tang WC, *Application of FRP Bars as Reinforcement in Civil Engineering Structures*. Structural Survey, 2002. **20**(2): p. 62-72.
4. 445, J.A.-A.C., *Recent Approaches to Shear Design of Structural Concrete (ACI 445R-99) (Reapproved 2009)*. 1999, Farmington Hills, MI: American Concrete Institute.
5. Wight, J.K., and MacGregor, J. G., *Reinforced Concrete: Mechanics and Design*. 7 ed. 2016, Upper Saddle River, NJ: Pearson Prentice Hall.
6. Abdul-Zaher, A.S., et al., *Shear Behavior of Fiber Reinforced Concrete Beams*. JES. Journal of Engineering Sciences, 2016. **44**(2): p. 132-144.
7. Al-lami, K.A., *Experimental Investigation of Fiber Reinforced Concrete Beams*, in *Civil and Environmental Engineering*. 2015, Portland State University. p. 118.
8. Maranan, G.B., et al., *Shear Behavior of Geopolymer Concrete Beams Reinforced with GFRP Bars*. ACI Structural Journal, 2017. **114**(2).
9. Mohamed S. Issa, H.M.I.a.E.-S.S., *BEHAVIOR AND MODELING OF CONCRETE DEEP BEAMS REINFORCED WITH GFRP REBARS*, in *1st International Conference on Innovative Building Materials*. 2014. p. 120-127.
10. A. Koray Tureyen, R.J.F., *Shear Tests of FRP-Reinforced Concrete Beams without Stirrups*. ACI STRUCTURAL JOURNAL, 2002. **99**(4): p. 428-434.
11. Abed, F., H. El-Chabib, and M. AlHamaydeh, *Shear characteristics of GFRP-reinforced concrete deep beams without web reinforcement*. Journal of Reinforced Plastics and Composites, 2012. **31**(16): p. 1063-1073.
12. Chen, H., et al., *Modeling of shear mechanisms and strength of concrete deep beams reinforced with FRP bars*. Composite Structures, 2020. **234**.
13. 440, A.C., *Guide for the Design and Construction of Externally Bonded FRP Systems for Strengthening Concrete Structures*. 2017, Farmington Hills, MI 48331: American Concrete Institute. 117.

نمذجة العناصر المحدودة غير الخطية لسلوك القص لعوارض الخرسانية العميقة المقواة بقضبان البوليمر المقوى بالألياف الزجاجية الداخلية بواسطة ANSYS

شعيب عبدالله محمد[1] – ماجستير
د. سيروان خورشيد رفيق[2] – استاذ مساعد
زانا عبدالله عزيز[3] – ماجستير
[3,2,1] جامعة السليمانية – كلية الهندسة – قسم الهندسة المدنية

المستخلص

يتزايد استخدام البوليمرات المسلحة بالياف الكربون (FRPs) ، والتي تتكون من ألياف كاربونية محقونة بمواد لاصقة صمغية، تستخدم البوليمرات المسلحة بالياف الكاربون بكثرة كبديل لحديد التسليح لتقوية الكمرات الخرسانية نظراً لسلوكها العالى فى تحسين مقاومة التآكل وقوة الشد والليونة. الهدف من هذا البحث هو التتبع العددي لاستجابة الكمرات الخرسانية العميقة المقواة بقضبان البوليمر المسلحة بالألياف الزجاجية (GFRP) وبدون تقوية الويب باستخدام برنامج العناصر المحدودة التجارية ANSYS.استخدمت نموذج العناصر المحدودة لكمرة خرسانية عميقة تم فحصها مسبقًا في دراسة تجريبية ومقارنة أحمال الفشل المتوقعة مع أحمال الفشل الفعلية. كانت نتائج نموذج العناصر المحدودة في توافق جيد مع النتائج المتحصلة من الدراسة العملية. أظهرت المقارنات أن النموذج المطور قادر على التقاط استجابة القص ، بالإضافة إلى استجابة انحراف الحمولة وأنماط الشقوق للحزم العميقة المقواة بقضبان البوليمر المسلحة بالألياف الزجاجية GFRP الداخلية في نطاق التحميل الكامل. كذلك تم خلال البحث أيضاً دراسة مفصلة حول نسبة امتداد القص إلى العمق (a / d) ، ونسبة التسليح للبوليمر المسلحة بالألياف الزجاجية GFRP وقوة ضغط الخرسانة التي عادةً ما يكون لها تأثيرات عالية على سلوك الكمرات الخرسانة المسلحة بالألياف. أظهرت نتائج الدراسة البارامترية أن حمل الفشل النهائي للعوارض المقواة بقضبان GFRP كان أعلى من عوارض الخرسانة المسلحة بالفولاذ. لوحظ أن الحمل الأقصى للفشل ينخفض عن طريق خفض نسبة a/d. حيث زادت صلابة وليونة الكمرات بزيادة نسبة التعزيز للبوليمر المسلحة بالألياف الزجاجية GFRP.

الكلمات المفتاحية:

الكمرات الخرسانية العميقة، البوليمرات المسلحة بألياف الكربون، نسبة امتداد القص إلى العمق (a / d)

14. AASHTO, *LRFD Bridge Design Specifications: SI Units*. 4 ed. 2007, Washington, DC: American Association of State Highway and Transportation Officials. 1596.
15. 318, A.C., *Building Code Requirements for Structural Concrete (ACI 318-19) and Commentary*. 2014, Farmington Hills, MI: American Concrete Institute. 473.
16. Matthias F. Andermatt, A.S.L., *Behavior of Concrete Deep Beams Reinforced with Internal Fiber-Reinforced Polymer—Experimental Study*. ACI Structural Journal, 2013. **110**(4): p. 585-594.
17. Ashour, A. and K.H. Yang, *Application of plasticity theory to reinforced concrete deep beams: a review*. Magazine of Concrete Research, 2008. **60**(9): p. 657-664.
18. *ANSYS, Inc., "ANSYS Help", Release 14.5.*
19. Amer M. Ibrahim, W.D.S., *FINITE ELEMENT ANALYSIS OF REINFORCED CONCRETE BEAMS STRENGTHENED WITH CFRP IN FLEXURAL*. Diyala Journal of Engineering Sciences, 2009. **2**(2): p. 88-104.
20. Sougata Chattopadhyay, R.R., N. Umamaheswari, *ANALYTICAL INVESTIGATION ON FLEXURAL BEHAVIOR OF CONCRETE BEAMS REINFORCED WITH GFRP REBARS*. International Journal of Civil Engineering and Technology (IJCIET), 2018. **9**(4): p. 1-8.

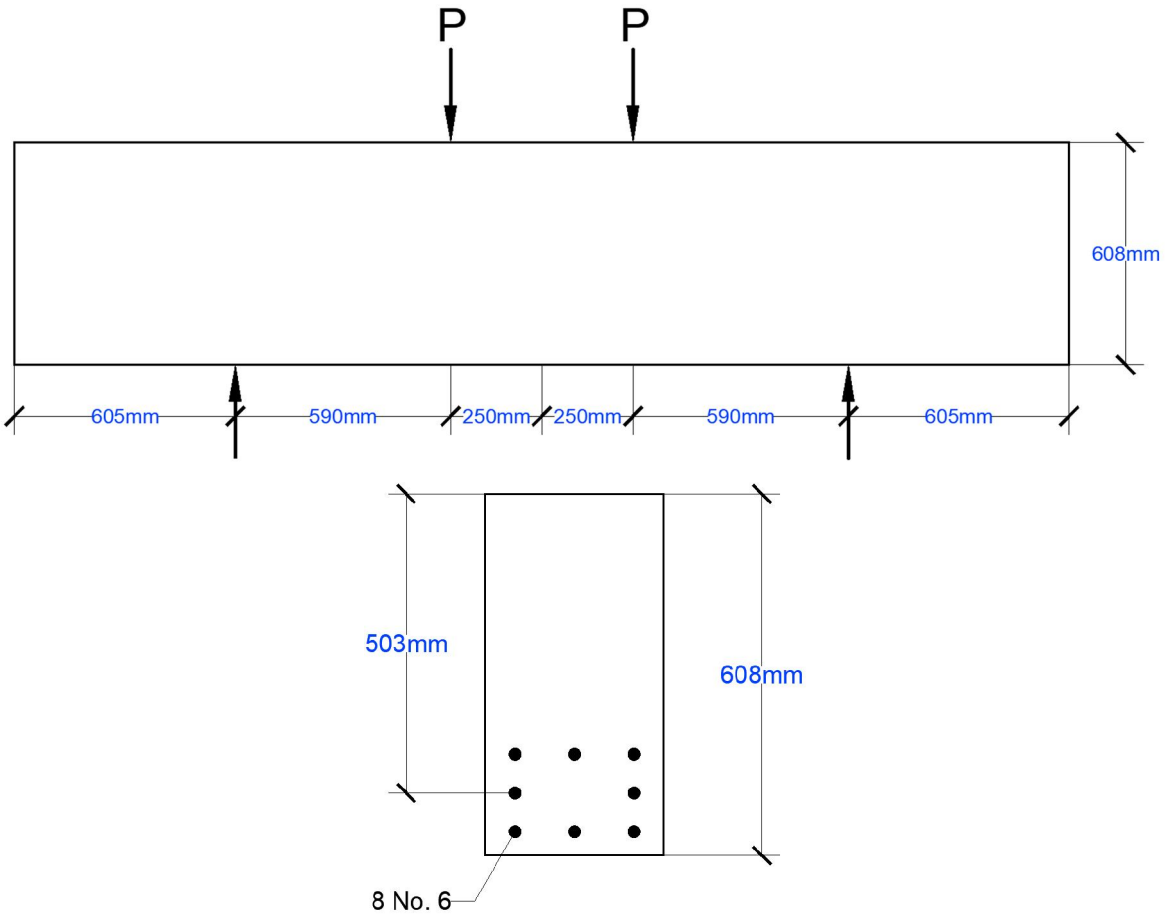

Fig. (1): Beam configuration and details of reinforcement (B1N) [16]

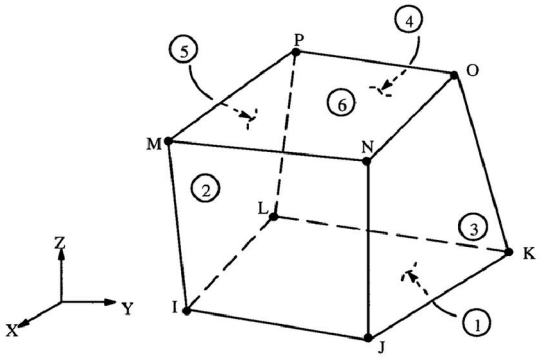

Fig. (2): Solid 65 Element Type [18]

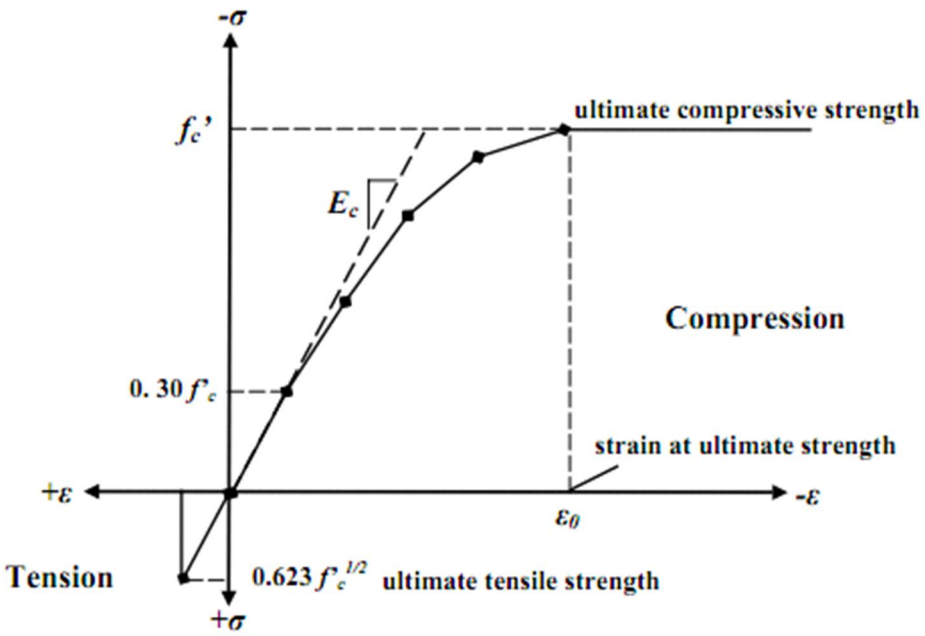

Fig. (3): Simplified compressive uniaxial stress-strain curve of Concrete

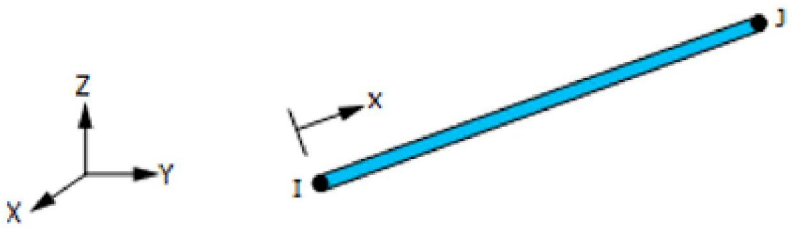

Fig. (4): Link 180 Element Type [18]

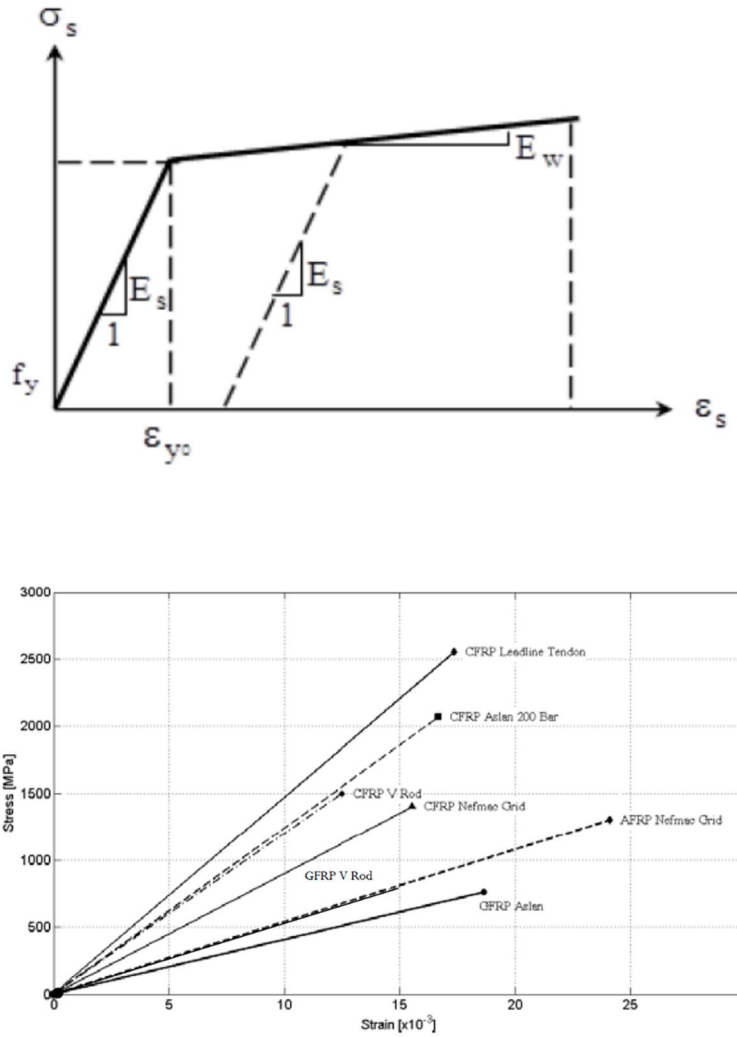

Fig. (5): Simplified stress-strain curve of Steel and FRP Materials [19]

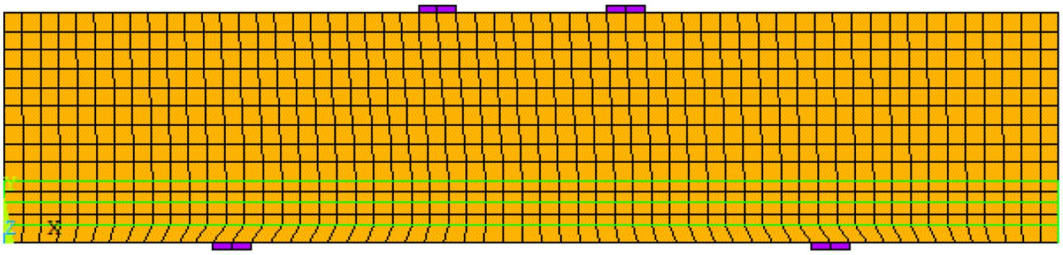

Fig. (6): Typical mesh of the finite element model of a beam B1N

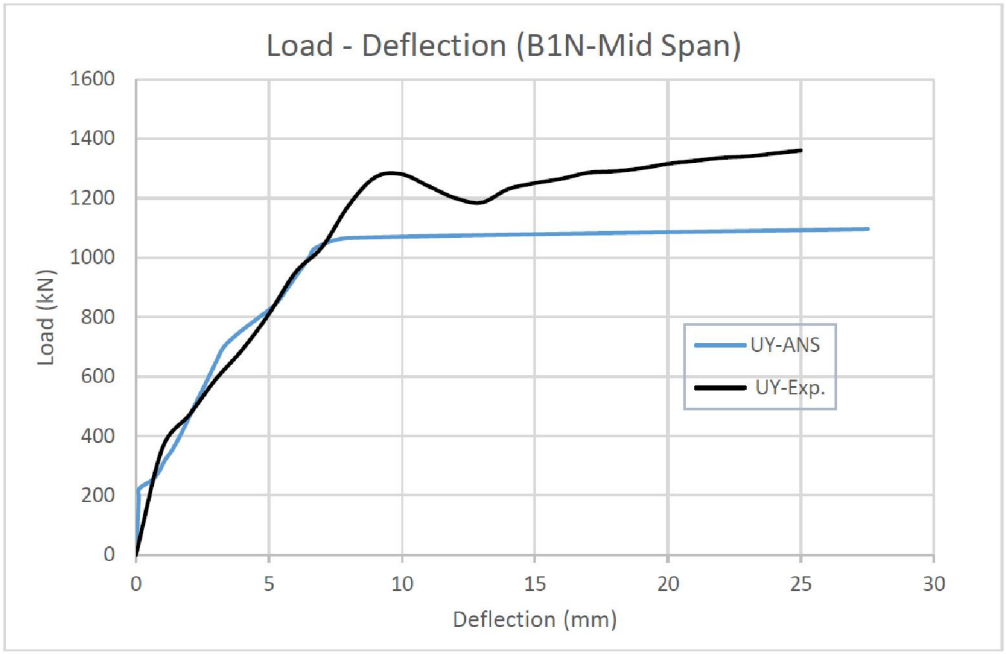

Fig. (7): Load-deflection response of beam B1N

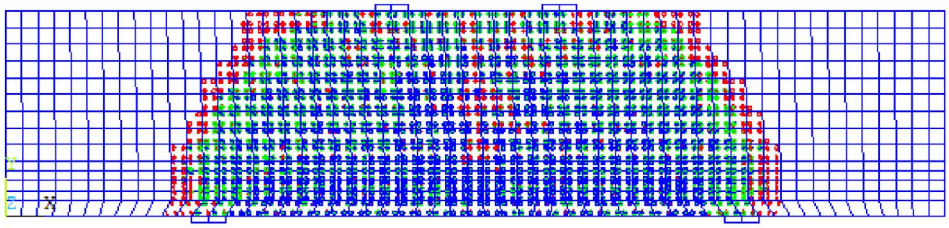

Fig. (8): Crack Pattern of beam B1N (a/d = 1.08)

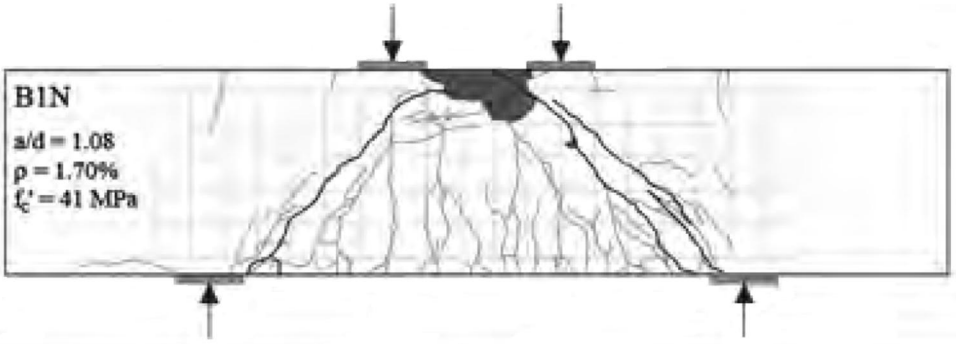

Fig. (9): Crack Pattern of beam B1N (Experimental Works) [16]

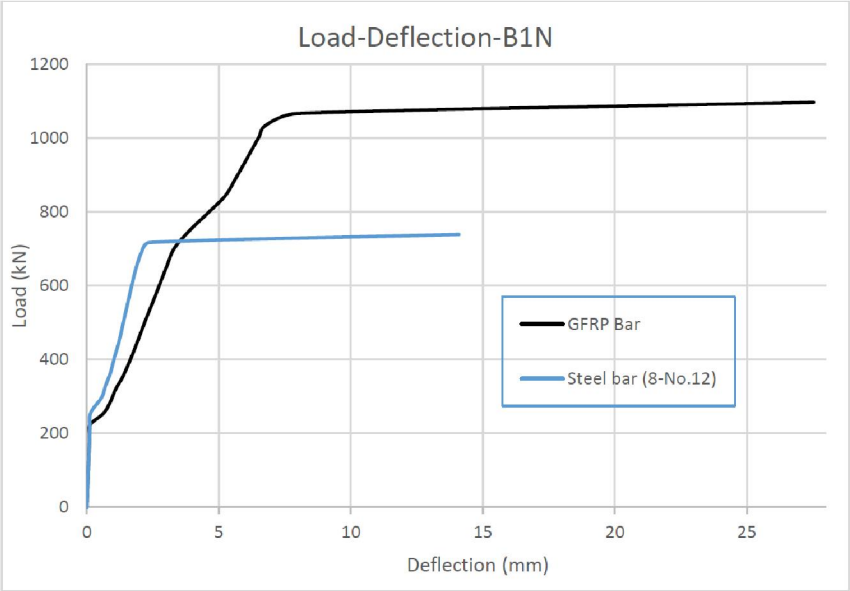

Fig. (10): Load-deflection of beams with GFRP and Steel bars

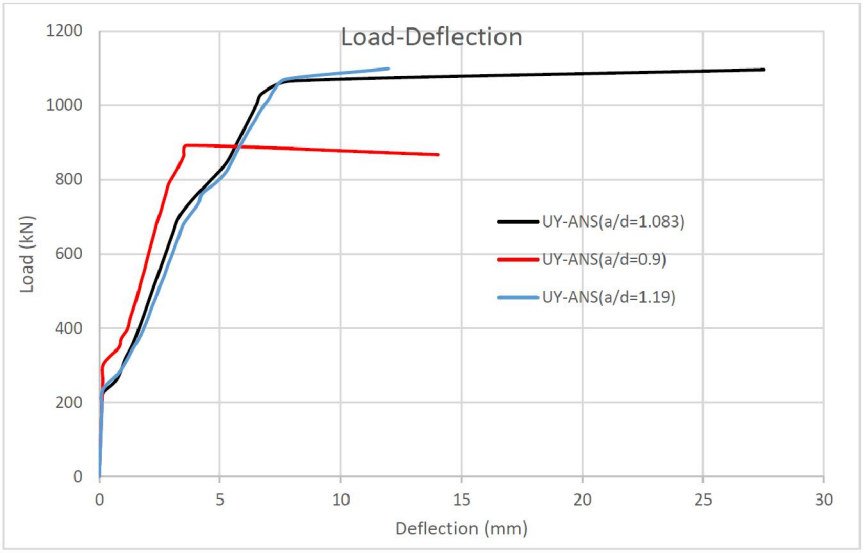

Fig. (11): Effect of different span-to-depth ratio for beam B1N

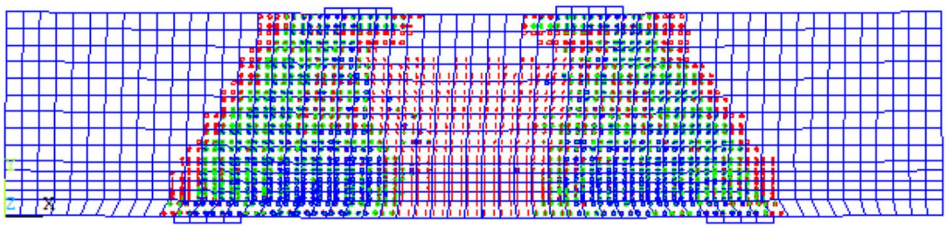

Fig. (12): Crack Pattern of beam B1N (a/d = 0.9)

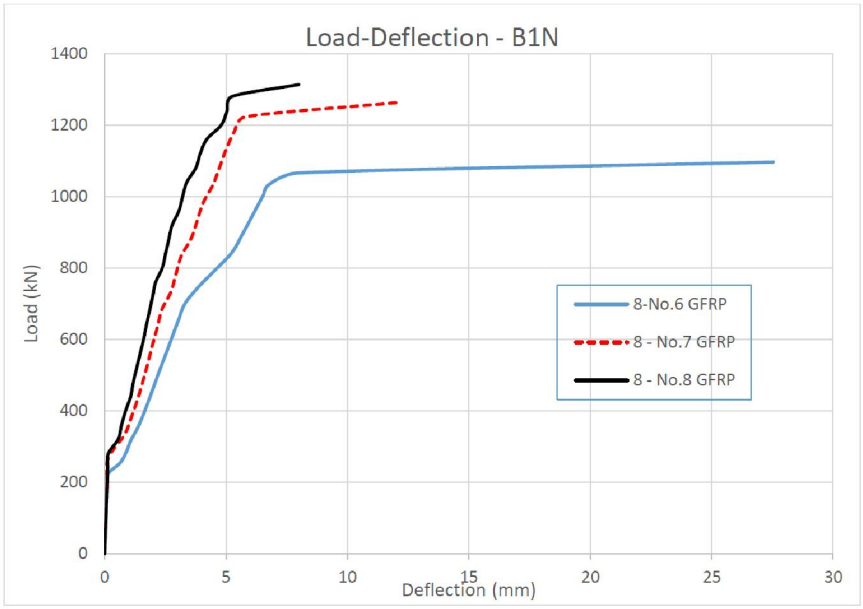

Fig. (13): Effect of different reinforcement ratio for beam B1N

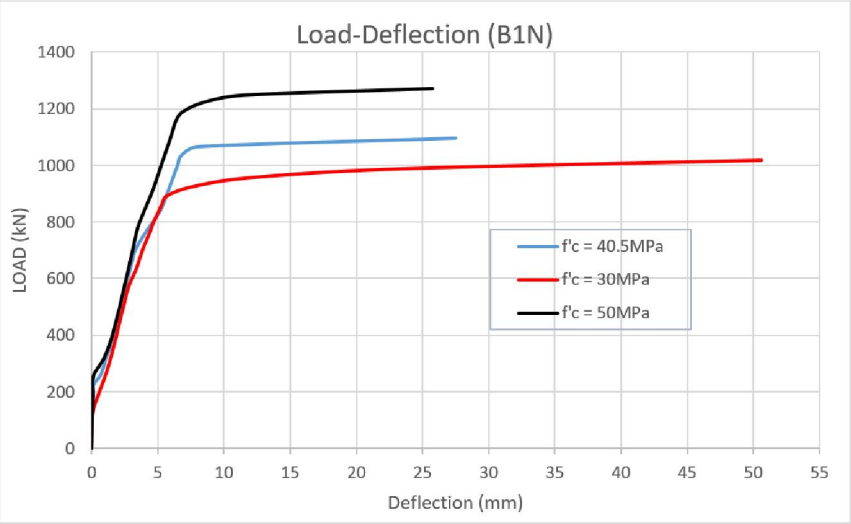

Fig. (14): Effect of different compressive strength for beam B1N (a/d = 1.08)

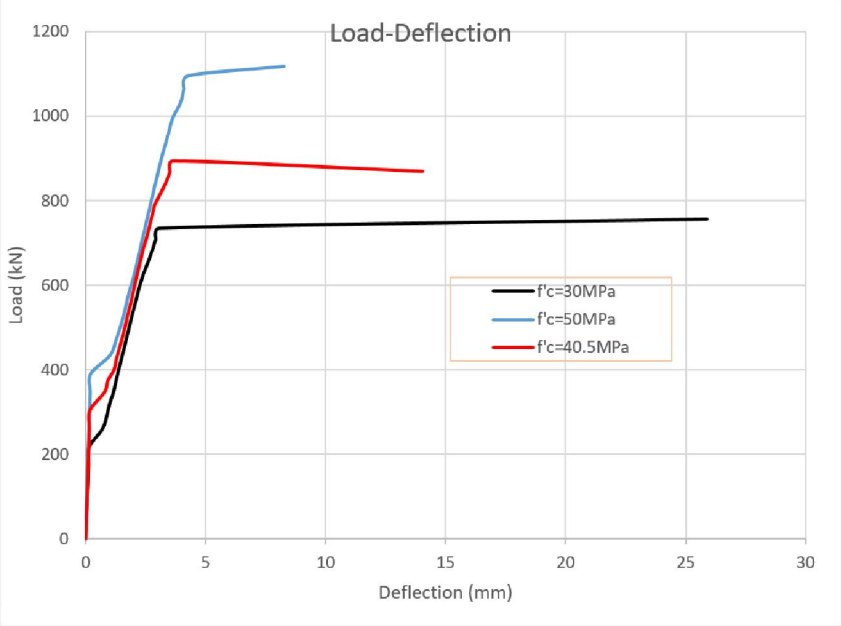

Fig. (15): Effect of different compressive strength (a/d = 0.9)

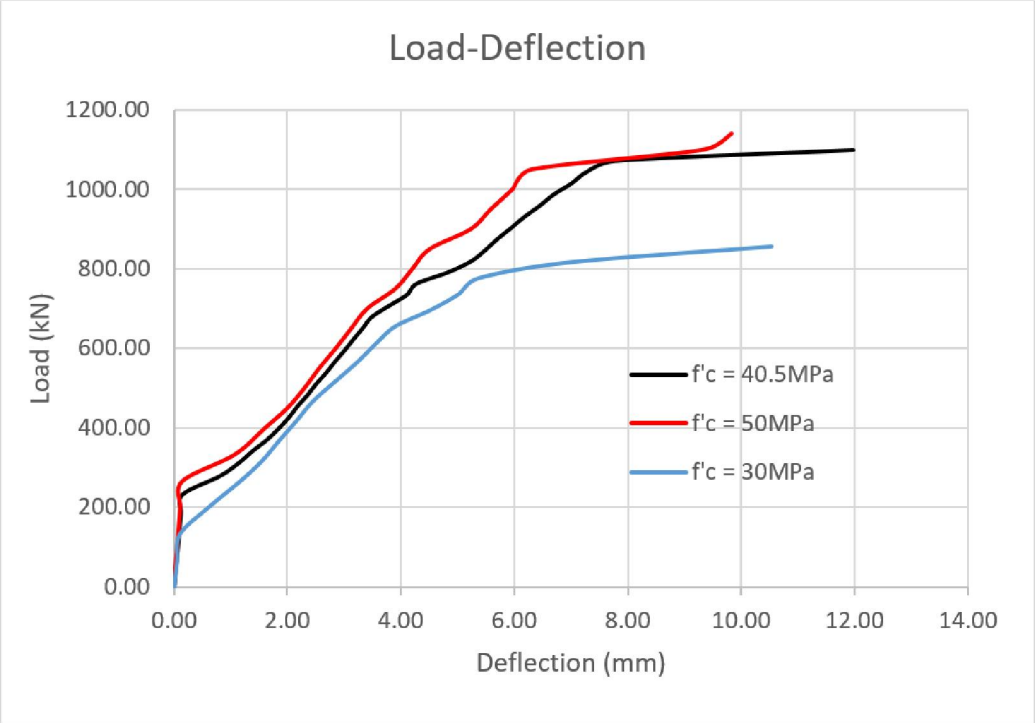

Fig. (16): Effect of different compressive strength (a/d = 1.19)

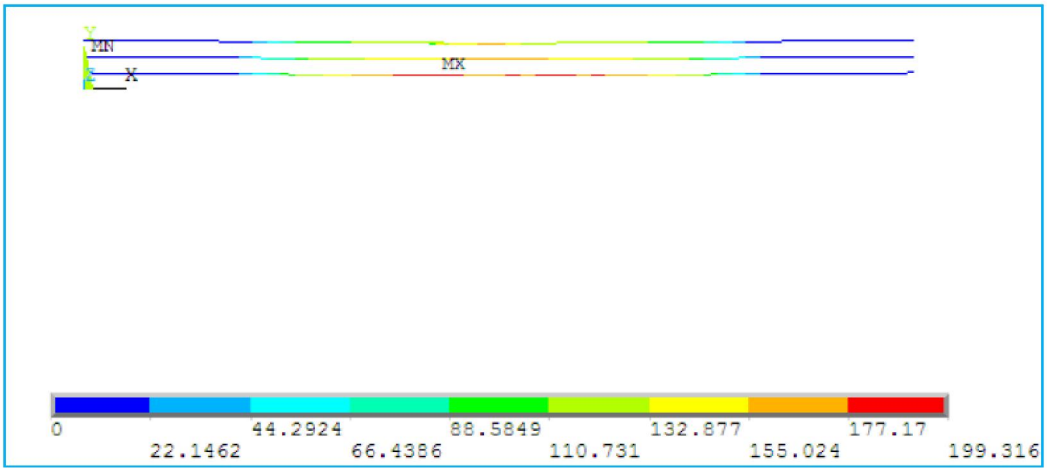

Fig. (17): Reinforcement Stresses for f'c = 30 MPa

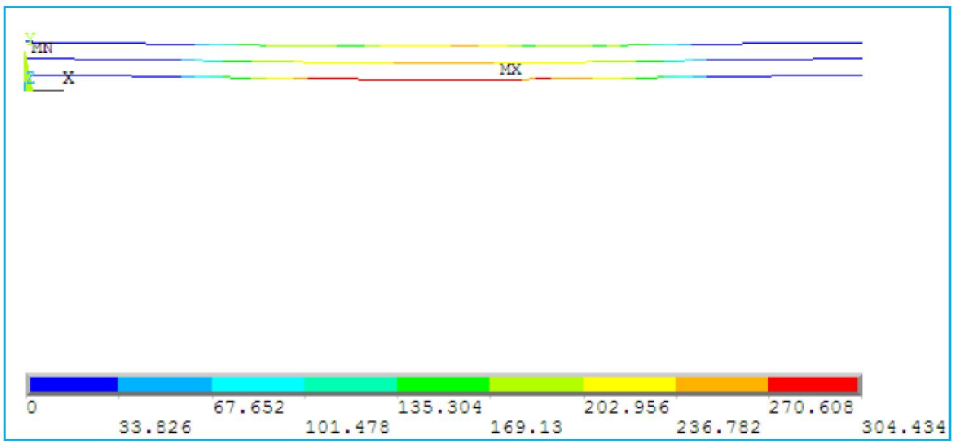

Fig. (18): Reinforcement Stresses for f'c = 40.5 MPa

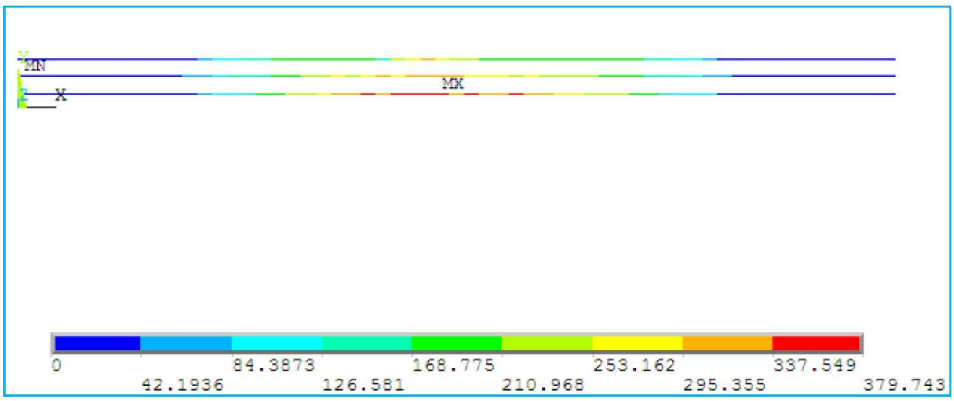

Fig. (19): Reinforcement Stresses for f'c = 50 MPa

Table (1) Properties of GFRP bars [16]

Reinforcement Property	Reinforcing bar size		
	No. 6 (19 mm)	No. 7 (22 mm)	No. 8 (25 mm)
Nominal Diameter, mm	19	22	25
Cross-sectional Area, mm²	322	396	528
Failure Stress, MPa	765	709	938
Modulus of Elasticity, GPa	37.9	41.1	42.3
Glass Content, % Vol.	72	64.8	64.1

Table (2) Cracking and Ultimate Load of GFRP- and Steel-Reinforced Concrete Deep Beams

Type of Beam	Pcr (kN)	Pu (kN)
Steel-reinforced Beam	252	741
GFRP-reinforced Beam	219	1097

Table (3) Cracking Load, Ultimate Load and Deflection at Failure of GFRP- Reinforced Concrete Deep Beams with Different Reinforcement Ratios

Reinforcement	Reinforcement Ratio (%)	Pcr (kN)	Pu (kN)	Deflection at Failure (mm)
8 No. 6	1.41	228	1096	27
8 No. 7	1.74	257	1262	12
8 No. 8	2.32	276	1312	8